Industrial Engineering and Innovation Management (2024)
Clausius Scientific Press, Canada

DOI: 10.23977/ieim.2024.070107
ISSN 2522-6924 Vol. 7 Num. 1

Research on Multi-view 3D Measurement Technology of Blade Based on Linear Structured Light

Zhang Haotian[a], Huang Danping[b,*], Wang Yijin[c]

College of Mechanical Engineering, Sichuan University of Science & Engineering, Yibin, 644000, China
[a]739047168@qq.com, [b]hdpyx2002@163.com, [c]619477291@qq.com
[*]Corresponding author

Keywords: Blade; 3D measurement; Multi-view; Line structured light; Global calibration

Abstract: For the precise three-dimensional measurement of the leaf contour of space engine blades, conventional measurement means cannot take into account the accuracy and completeness of the measurement, this paper proposes a multi-view measurement system based on line structured light and a global optimisation method to improve the blade measurement accuracy. Firstly, the multi-view simultaneous acquisition of blade deformation profile images is completed by a multi-camera acquisition system, and the multi-view system is globally coordinate unified by using the complete global calibration of four sets of binocular subsystems. Then, a global optimisation method is proposed to perform ICP point cloud alignment on the point clouds of neighbouring views in the high overlap region, while the global calibration of cylindrical calibrators is completed for non-neighbouring views, and cylindrical fitting is performed through the geometrical features of the calibrators in order to complete the secondary optimisation. The experimental results show that the average standard deviation of the method is 0.1253 mm for the blade, which meets the actual inspection requirements.

1. Introduction

Blade is the core component of aero-engine, and its profile measurement is a key step in reverse engineering, quality inspection, blade design and repair, so the 3D measurement technology of blade profile has been a research hotspot[1][2]. The three-dimensional measurement techniques of the blade are usually divided into two categories: contact and non-contact measurement[3][4]. The contact measurement acquires the three-dimensional information on the surface of the object by directly contacting the object to be measured. This measurement method has the advantages of high accuracy and reliability, but also has the disadvantages of long measurement time, low efficiency, and easy to damage the probe and the object to be measured, etc. The Non-contact Measurement acquires the three-dimensional morphology of the surface of the object to be measured through the acoustic, optical, and electromagnetic methods, which are mainly ultrasonic ranging, Structured light method, industrial CT and other methods, non-contact measurement methods both high-speed and high-efficiency advantages, in recent years has been widely used in a variety of industrial inspection environment[5][6][7]. The complexity of the blade profile requires high measurement

accuracy and integrity, and there is no universal measurement method with both high accuracy and high integrity.

Line structured light three-dimensional measurement technology in non-contact is one of the important means of blade measurement at present because of its features such as high measurement accuracy, fast speed, high point cloud density, etc., which can satisfy the measurement needs of blade profiles, and the cost of measurement is lower than most of the three-dimensional measurement technologies. However, there are still some challenges to achieve high-precision 3D measurement of the whole surface of the blade based on line structured light technology.

(1) A single line of structured light 3D measurement system can only obtain the 3D information of a certain angle of the blade at a single time, which cannot meet the requirements of the integrity of the blade measurement.

(2) The blade point cloud data obtained from multiple viewpoints need to unify the coordinate systems of each viewpoint to obtain a complete blade surface profile. Currently, the commonly used method is global calibration[8][9], but due to the calibration plate error and the limitations of the calibration algorithm, the point cloud is still misaligned and layered after the global unification of the coordinate system in each viewpoint.

Aiming at the above problems, this paper designs and builds a three-dimensional measurement system for multi-view line structured light blades, obtains high-precision measurement point cloud data in each view angle of the blade, and then realises high-precision splicing and fusion of blade point cloud data in multiple view angles by the global calibration method proposed in this paper. The method firstly uses the global calibration principle to unify the global coordinates of the point clouds located in different coordinate systems, and then completes the high-precision profile reconstruction of the whole surface of the blade through the global calibration error compensation.

2. Multi-viewing angle line structured light measurement system construction

The structure of the whole multi-view line structured light 3D measurement system is shown in Figure 1. The system consists of a computer, an industrial camera, a line laser, a servo displacement module, and an electrical control box. In this system, the computer is used to control the servo displacement module, and according to the set target speed and position, the computer runs the guide rail to the specified position. At the same time, the system computer also controls four industrial cameras for shooting during motion, and the software for related algorithms is implemented internally. During the operation of the object, the line laser projects structured light onto the measured blade, covering the entire measured object with the structured light image. At this time, four industrial cameras complete the capture of the deformation stripe image of the measured object, forming a complete measurement system process.

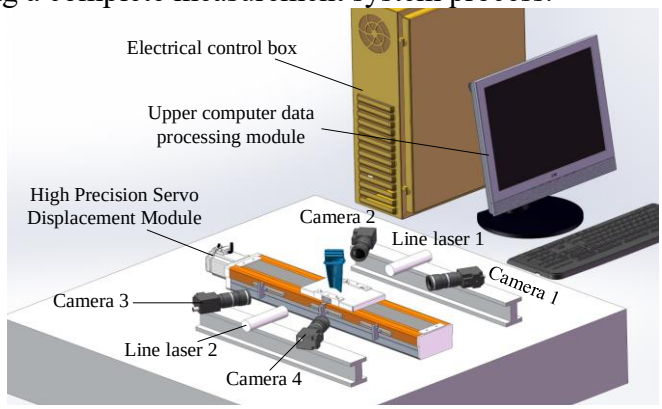

Figure 1: Multi-view line structured light 3D measurement system

The working principle of the system is shown in Figure 2. Four cameras are distributed around the object under test, and the two cameras on the same side share a line laser. Through the movement of the object under test, the structured light projected by each line laser can cover the field of view of the two cameras on the same side. $\pi_1, \pi_2$are the structured light planes projected by the two line lasers, $P_1, P_2$is the points on the intersection line between the two light planes and the object under test, the world coordinate system, the camera coordinate system of camera No. i. Camera 1 is selected as the master camera, and cameras 2, 3, and 4 are the slave cameras; the master camera 1 and the light plane π_1 constitute the line structured light measurement unit 1, and the slave camera 2 and the light plane π_1 constitute the line structured light measurement unit 2, and the slave camera 3 and the light plane π_2 The line structure light measurement unit 3 is composed of the line structure light measurement unit 3, the slave camera 4 and the light plane π_2 is composed of the line structure light measurement unit 4, H_{i1} denoting the transformation matrix of i number from the coordinate system of the camera to the master camera 1 coordinate system, then the overall measurement idea is as follows: first, each measurement unit carries out the local measurement and then the global splicing of the locally measured point cloud data. The specific steps are:

(1) Each measurement unit performs local measurements according to the principle of monocular line structured light 3D measurement to achieve accurate measurements in the respective camera coordinate system for each viewpoint ;

(2) Transform the slave camera coordinate system to the master camera coordinate system according to the selected master-slave camera relationship. The master camera 1 coordinate system is used as the global coordinate system, and the transformation matrix from the slave camera coordinate system to the master camera 1 global coordinate system is calculated for number i .

$$P_{C1} = H_{i1}P_{Ci} \tag{1}$$

Unify the local coordinate system to the global coordinate system by using the calculated transformation matrix to achieve global stitching of the point cloud data of the local measurement unit, so as to obtain the measurement results of the whole surface of the measured object;

$$\begin{cases} Z_{Ci}P_i = A_iP_{Ci} \\ a_iX_{Ci} + b_iY_{Ci} + c_iZ_{Ci} + d_i = 0 \; i \in \{1,2,3,4\} \\ P_{C1} = H_{i1}P_{Ci} \end{cases} \tag{2}$$

In summary, the mathematical model of the multi-view 3D measurement system for leaves based on line structured light is shown below:

Where i denotes the number of the camera, $Z_{Ci}P_i = A_iP_{Ci}$ denotes the imaging model of camera i, Z_{Ci} is the scale factor of camera i, $a_iX_{Ci} + b_iY_{Ci} + c_iZ_{Ci} + d_i = 0$ denotes the equation of the light plane in the coordinate system of each camera, $a_ib_ic_id_i$ is the physical parameters of the light plane in the coordinate system of camera i, P_i denotes the two-dimensional image coordinates of point P of camera i, P_{Ci} denotes the three-dimensional coordinates of camera i for the point P, A_i denotes the projection matrix of camera i, and H_{i1} denotes the transformation matrix of the coordinate system of camera i to the coordinate system of camera 1.

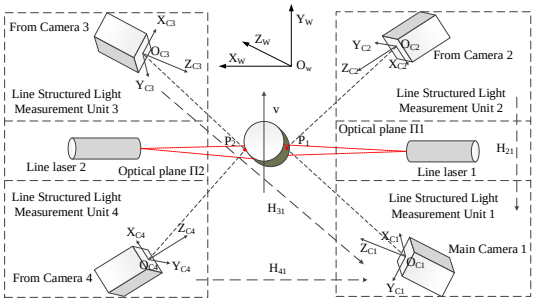

Figure 2: Multi-viewing angle line structured light 3D measurement system model

3. Calibration of multi-view line structured light measurement system

The calibration of the multi-viewing angle line structured light measurement system is mainly divided into two parts: one is the local calibration of each line structured light measurement unit, which acquires the camera parameters, optical plane parameters and scanning direction parameters of each line structured light measurement unit; the other is the global calibration of the multi-viewing angle line structured light measurement system, which unifies the local measurement data acquired by the line structured light sensors into the global coordinates to achieve the global splicing of the measurement data. Regarding the calibration of single-line structured light measurement system is now quite mature, and will not be repeated in this paper.

3.1 Global calibration

In the multi-view line structured light three-dimensional measurement system constructed in this paper, the two adjacent cameras meet the requirements of binocular stereo vision construction, then it can be composed of four groups of binocular sub-systems, as shown in Figure 3. In the binocular sub-systems composed of the two adjacent cameras, the checkerboard grid calibration plate is placed in the overlapping field of view of the two adjacent binocular sub-systems, and the position of the calibration plate is constantly changed. The two cameras respectively collect the images of the calibration plate in different positions, and the image of the calibration plate can be solved through the principle of binocular calibration. Through the principle of binocular stereo calibration, the transformation relationship between the coordinate systems of two neighbouring cameras can be solved.

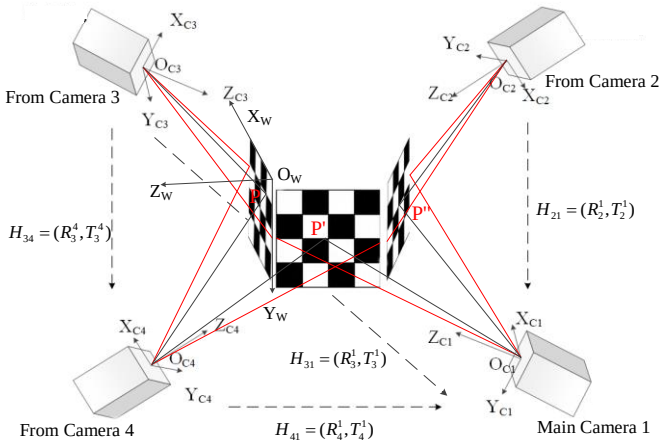

Figure 3: Principle of global calibration of multi-view camera coordinate system

Assuming that the point P is a corner point of the checkerboard grid calibration board, its

coordinates under the calibration board coordinate system are $P_W = (X_W, Y_W, Z_W)$, its coordinates under the slave camera 3 coordinate system are P_{C3}, its coordinates under the slave camera 4 coordinate system are P_{C4}, the transformation matrix from the calibration board coordinate system to the slave camera coordinate system 3 is $H_{w3} = (R_w^3, T_w^3)$, and the transformation matrix from the calibration board coordinate system to the slave camera coordinate system 4 is $H_{w4} = (R_w^4, T_w^4)$, then we can obtain the following equation:

$$\begin{cases} P_{C3} = R_w^3 P_w + T_w^3 \\ P_{C4} = R_w^4 P_w + T_w^4 \\ P_{C4} = R_3^4 P_{C3} + T_3^4 \end{cases} \tag{3}$$

Where, $H_{34} = (R_3^4, T_3^4)$ is the relationship matrix for the transformation from camera 3 coordinate system to from camera 4 coordinate system, the simplification of equation (3) yields the following equation (4):

$$\begin{cases} R_3^4 = R_w^4 \cdot (R_w^3)^T \\ T_3^4 = T_w^4 - R_3^4 T_w^3 \end{cases} \tag{4}$$

The transformation matrix $H_w^3 = (R_w^3, T_w^3)$, $H_w^4 = (R_w^4, T_w^4)$, and thus the relation matrix $H_{34} = (R_3^4, T_3^4)$for the transformation from the camera 3 coordinate system to that from the camera 4 coordinate system can be obtained by calibrating the external parameters of the camera according to Eq. (4).

Similarly, the binocular subsystem composed of the slave camera 4 and the master camera 1, and the slave camera 2 and the master camera 1 is calibrated, and the transformation matrix $H_{41} = (R_4^1, T_4^1)$ from the coordinate system of the camera 4 to the coordinate system of the master camera 1 can be obtained, the transformation matrix $H_{21} = (R_2^1, T_2^1)$ from the coordinate system of the camera 2 to the coordinate system of the master camera 1 can be obtained by the transformation of the coordinate system from the coordinate system of the camera 3 to the coordinate system of the master camera 1 is shown in Equation (5).

$$H_{31} = H_{34} \bullet H_{41} \tag{5}$$

Therefore, according to the global calibration results H_{21}, H_{31}, H_{41} , it is possible to globally unify the local coordinate system from cameras 2, 3 and 4 to the global coordinate system of the main camera 1, so as to realise the global stitching of the measurement point cloud under the local coordinate system of each measurement unit.

3.2 Global calibration optimization

In the process of transforming from the local coordinate system of the camera to the global coordinate system of the main camera, the coordinate system of camera 3 needs to be transformed to the coordinate system of camera 4 first, and then transformed to the global coordinate system where the main camera 1 is located. The transformation process is the result of the cumulative multiplication of the transformation matrix. Therefore, the cumulative error gradually increases in the process of transforming from the coordinate system of camera 3. In addition, due to the manufacturing accuracy of the calibration plate and the limitations of the calibration algorithm, the error in global calibration is caused, resulting in the increase of the global splicing error of the measured point cloud, which is manifested as the layered misalignment of the fused point cloud. In addition, due to the manufacturing accuracy of the calibration plate and the limitations of the calibration algorithm and other factors will lead to the global calibration error, making the global splicing error of the measurement point cloud increase, which is manifested as the layered

misalignment of the fused point cloud[10][11], and the real 3D size of the measured object cannot be measured accurately. Therefore, it is necessary to carry out the secondary optimisation of the measurement system after global calibration, which can effectively reduce the impact of the transformation matrix multiplication and calibration errors, so as to achieve the accurate splicing of point cloud data[12][13].

Based on this, a splicing optimisation scheme applicable to the blade measurement point cloud in this paper is proposed for the precise splicing demand of multi-view point cloud data. As shown in Figure 4, the field of view distribution of the multi view blade 3D measurement system constructed in this article is overlapping between adjacent cameras. Due to the unique structure of the blades, there is a partial overlap in the field of view (OFOV) between the main camera 1 and the secondary camera 2, as well as between the secondary camera 3 and the secondary camera 4, while there is less overlap in the field of view between the secondary camera 4 and the main camera 1. Therefore, both Line Structured Light Measurement Units 1 and 2 and Line Structured Light Measurement Units 3 and 4 have some common measurement point clouds, while Line Structured Light Measurement Units 4 and 1 have fewer or even no common measurement point clouds. In view of this, this paper adopts different splicing optimization methods for two-frame point clouds with overlapping regions and point clouds without overlapping regions, as shown in Fig. 5, and uses the point cloud alignment algorithm to make point clouds with overlapping regions overlap completely; for point clouds without overlapping regions or point clouds with fewer overlapping regions cannot be optimized by using the point cloud alignment algorithm to perform the global alignment optimization, and this paper proposes the use of cylindrical samples for the optimisation.

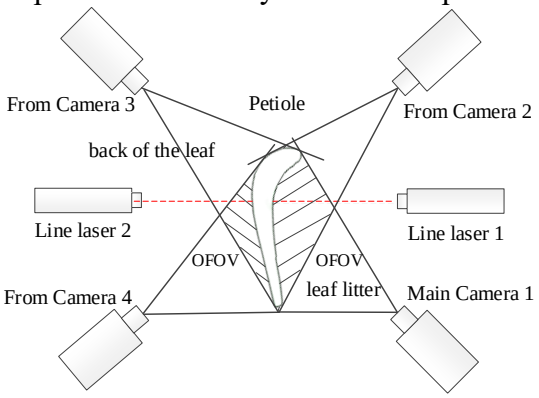

Figure 4: Distribution of the field of view of the multi-view 3D measurement system

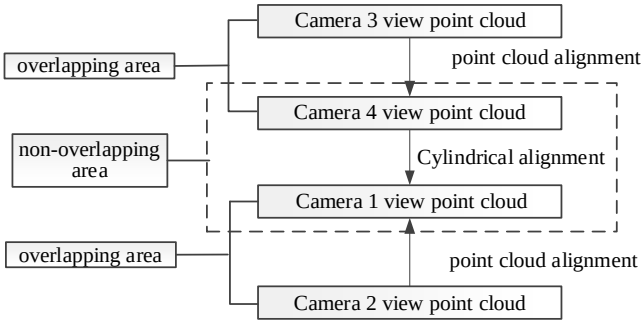

Figure 5: Global calibration optimisation scheme

3.2.1 Global calibration optimisation of local overlapping regions

Accurate stitching of point cloud data with locally overlapping regions using point cloud alignment algorithms to achieve complete overlap and reduce global calibration errors.

The most widely used point cloud alignment algorithms are and their improvements[14]. The steps of the traditional ICP algorithm are as follows:

(1) Assuming that the source point cloud set is $s = (s_1, s_2, s_3, \ldots s_n)$and the target point cloud set is T $= (t_1, t_2, t_3, \ldots t_n)$, find the corresponding point in the source point cloud set S that has the closest relative distance to the target point cloud set T. Where is the number of corresponding points in the target point cloud set and source point cloud set, k is the number of iterations, and R and T are the rotation and translation matrices calculated in each iteration.

$$P_i^k = \min \parallel R^{k-1} \cdot t_n - T^{k-1} - s_n \parallel^2 \tag{6}$$

(2) According to the following objective function equation (5-5), the optimal solution of the rotation translation matrix R^k, T^kcan be obtained by optimisation using the least squares method.

$$f(R^k, T^k) = min \sum_{i=1}^{n} \parallel R^k \cdot t_n \tag{7}$$

(3) The calculated rotational translation relation is transformed to the source point cloud set S with the transformation equation:

$$P_i^{k+1} = R^k \cdot s_n + T^k \tag{8}$$

(4) Calculate the mean Euclidean distance D^{k+1}between the transformed source and target point clouds.

$$D^{k+1} = \frac{1}{i} \Sigma_{a=1}^{i} \parallel s_n - t_n \parallel^2 \tag{9}$$

(5) If D^{k+1} is less than the given distance threshold τor reaches the set number of iterations, the algorithm ends, otherwise return to step (1) and repeat the above steps until the convergence condition is satisfied. At this point, the ICP algorithm can be used to solve the global calibration optimisation matrix ΔH_{21} ,ΔH_{34} between cameras 1 and 2 and cameras 3 and 4, which compensates for the error in the global calibration results and improves the accuracy of point cloud stitching.

3.2.2 Global calibration optimisation for non-overlapping regions

In the previous section, the secondary optimisation of point cloud splicing for line structure light measurement units 1 and 2 and line structure light measurement units 3 and 4 has been completed, and then the splicing optimisation of point cloud of line structure light measurement units 4 and 1 can be done to complete the accurate fusion of the global point cloud. Due to the special characteristics of the blade structure, the point cloud data acquired by the line structure light measurement units 4 and 1 have fewer or even no overlapping regions, so using the improved ICP algorithm to accurately stitch these two frames of point cloud cannot achieve the purpose of global calibration secondary optimisation of the non-overlapping regions.

In view of this, this paper proposes a secondary optimisation of the measurement system after global calibration using 3D calibrators. Since the cylindrical shape has the same curvature at every angle, the global calibration is optimised using cylindrical samples for the non-overlapping region point clouds, and the appearance of the cylindrical parts is shown in Fig. 6.

Figure 6: Appearance of cylindrical parts

The steps of the algorithm are as follows:

(1) The cylindrical sample shown in Fig. 6 is placed in the overlapping field of view of cameras 1 and 4, and the multi-view line structured light 3D measurement system constructed in this paper is used to reconstruct the point cloud data of the surface morphology of the cylindrical sample in each view angle, and the four frames of the point cloud data are united by the global calibration results into the global coordinate system where camera 1 is located.

(2) According to the results of the global calibration optimisation of the local overlapping region, the point cloud data acquired by cameras 1 and 2 and cameras 3 and 4 are secondarily optimised to achieve accurate splicing of the local point clouds.

(3) Use the cylindrical fitting algorithm in the PCL library to fit cylinders to the fused two-piece point clouds P21,P34, respectively, and calculate the axial vectors $\overrightarrow{n_1}, \overrightarrow{n_2}$ of the two cylinders, as well as the centroid coordinates of the bottom circles of the two cylinders $S_1(X_1, Y_1, Z_1)$,$S_2(X_2, Y_2, Z_2)$.

(4) Under the global coordinate system, take the axis $\overrightarrow{n_1}$of the fused point cloud P21 of cameras 1 and 2 as the reference, and calculate the transformation relationship matrix between the axis of the fused point cloud P34 of cameras 3 and 4 and the transformation relationship matrix between the axis of the fused point cloud P34 of cameras 3 and 4, which is calculated as shown in Equation (10).

$$\begin{cases} \overrightarrow{n_1} = R_{12} \cdot \overrightarrow{n_1} \\ T_{12} = S_1 - S_2 \end{cases} \tag{10}$$

Where $R_{12}, T_{12}$is the rotation translation matrix of the axis $\overrightarrow{n_2}$ to $\overrightarrow{n_1}$direction transformation. By the above method, we can obtain the global calibration correction matrix $\Delta H_{41}$from the coordinate system of camera 4 to the coordinate system of master camera 1, and then the transformation relation between the coordinate system of camera 3 and the coordinate system of master camera 1 is shown as follows:

$$H_{31} = H_{34} \cdot \Delta H_{34} \cdot H_{41} \cdot \Delta H_{41} \tag{11}$$

Where ΔH_{34} is the correction matrix for the global calibration of cameras 3 and 4, which is calculated from the optimisation of the global calibration of locally overlapping regions in the previous section. The obtained correction matrix between the slave camera 4 coordinate system and the master camera 1 coordinate system corrects the global calibration error, realises the secondary optimisation of the global calibration of the point cloud in the non-overlapping region, and achieves the accurate splicing of the global measurement point cloud data.

4. Experimental validation and result analysis

In this paper, an aero-engine turbine blade is selected as the measurement object to verify the feasibility and validity of the proposed method, as shown in Fig. The appearance of the blade, with a chord length of 40 mm, is shown in Fig. 4. Four baumer cameras with 2048×1536 pixels and 8 mm focal length lenses are used to construct a set of multi-viewing angle line structured light three-dimensional measurement system, and the practicality of the proposed method is verified, as shown in Fig. 7. The practicality of the proposed method is shown in Fig. 7. In the constructed multi-view line structured light 3D measurement system, the camera and the lasers are arranged in a direct-type layout, and the lasers are vertically irradiated to the surface of the object to be measured, forming an angle of 40° with the optical axis of the camera. A simple checkerboard grid target can complete the calibration of the system parameters, the selected checkerboard grid target corner spacing of 6mm, the number of horizontal and vertical angle points of 11 × 8, as shown in Figure 8.

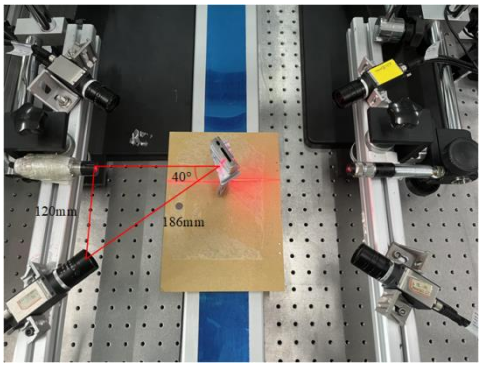

Figure 7: Physical diagram of the multi-view line structured light 3D measurement system

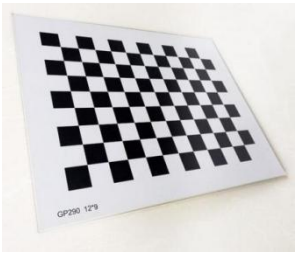

Figure 8: Tessellated calibration board

According to the global calibration principle described in the previous section, the checkerboard grid target is sequentially placed in at least three different positions within the overlapping field of view of the neighbouring cameras, and the neighbouring cameras acquire checkerboard grid images at different positions, and the chi-square transform matricesH_{21},H_{41}, and the chi-square transform matrix from the slave camera 4 and from the slave camera 2 to the master camera 1, and the chi-square transform matrices$H_{34}$of the slave camera 3 to the slave camera 4, with the results as shown below, are obtained with the Zhang Zhengyou camera calibration method[15]:

$$\begin{bmatrix} 0.4749 & -0.0203 & -0.8798 & -183.9827 \\ 0.0112 & 0.9998 & -0.0170 & 6.4063 \\ 0.8799 & -0.0018 & 0.4751 & 107.6480 \\ 0 & 0 & 0 & 1 \end{bmatrix} \tag{12}$$

$$\begin{bmatrix} 0.7492 & 0.0250 & -0.1324 & -197.3416 \\ -0.0073 & 0.9993 & 0.0150 & 5.1091 \\ -0.3254 & -0.1006 & 0.9249 & 18.4280 \\ 0 & 0 & 0 & 1 \end{bmatrix} \tag{13}$$

$$\begin{bmatrix} 0.2911 & -0.0028 & -0.9567 & -181.1104 \\ 0.0050 & 1.0000 & -0.0045 & -1.2869 \\ 0.9567 & -0.0061 & 0.2911 & 148.6864 \\ 0 & 0 & 0 & 1 \end{bmatrix} \tag{14}$$

Therefore, according to the global calibration resultsH_{21}, H_{41}, H_{34} , it is possible to globally unify the local coordinate system from cameras 2, 3 and 4 to the global coordinate system of the main camera 1, so as to realise the global stitching of the measurement point cloud under the local coordinate system of each measurement unit.

4.1 Global calibration optimisation

After the global calibration is performed on the multi-view line structured light 3D measurement

system, the accuracy of the global calibration needs to be verified, and for this purpose, measurement experiments of the standard parts are carried out. According to the global calibration results, the coordinate system of the point cloud acquired by the four measurement units is globally unified, so as to realise the global splicing of the four frames of the point cloud, as shown in Fig. 9(a). From Fig. 9(b), it is not difficult to find that the splicing of the two frames of point cloud without global calibration optimisation appears the phenomenon of splicing delamination and misalignment, so this paper proposes a secondary optimisation scheme for the phenomenon which is very necessary.

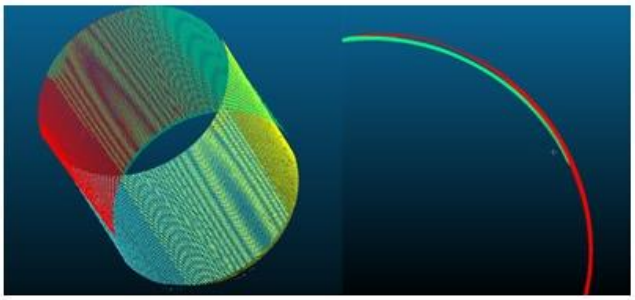

(a) Point cloud coarse splicing (b) point cloud coarseness

Figure 9: Multi-view coordinate system global coordinate system unification

The global calibration optimisation method proposed in this paper is divided into two steps, firstly, according to the scanning results of the four line structured light measurement units, the ICP algorithm is used to accurately stitch the point clouds of Cameras 1, 2 and Cameras 3, 4 with overlapping regions to obtain the point cloud data P_{21},P_{34}, and then the fused point clouds P_{21},P_{34} without overlapping regions are secondly calibrated by using the cylindrical samples to ultimately realise the accurate splicing of the point cloud data in different viewing angles.

The fused point clouds P_{21}, P_{34} after accurate stitching of the cylindrical sample point cloud data after global calibration using the ICP algorithm are shown in Fig 10.

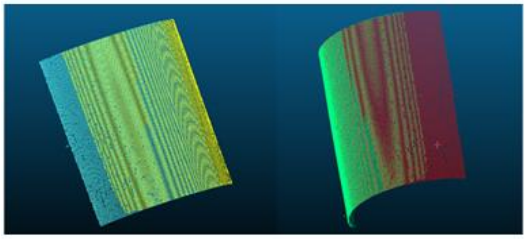

(a) point cloud fusionP21 (b) point cloud fusionP34

Figure 10: Point cloud optimisation results for local overlapping regions

Cylindrical fitting is performed for the fused point clouds P_{21} and P_{34} to obtain the cylindrical axis parameters as shown in Table 1.

Table 1: Cylindrical axis parameters

Coordinates of the centre of the circle on the bottom surface	axis direction vector
P_{21}=(-18.8751,-88.7987,35.8417)	$\overrightarrow{n_{21}}$ =(0.0814,0.9967,0.0065)
P_{34}=(-18.0372,-87.6832,34.8753)	$\overrightarrow{n_{34}}$ =(0.0873,1.0004,0.0050)

From the above table, it can be seen that the four camera coordinate systems after global

calibration have been coarsely spliced with each other, and the cylindrical axis vectors fitted to the fused point clouds P_{21} and P_{34} are very close to each other. The rotational and translational relationships between the fused point clouds P_{21}, P_{34} are calculated according to the previously derived Eq. (5-9) and are obtained:

The rotation and translation matrix between the fused point cloud P_{21}, P_{34} is:

$$T = \begin{bmatrix} X_2 - X_1 \\ Y_2 - Y_1 \\ Z_2 - Z_1 \end{bmatrix} = \begin{bmatrix} -0.8379 \\ -1.1155 \\ -0.9664 \end{bmatrix}, R = \begin{bmatrix} 1.0000 & -0.0056 & -0.0002 \\ 0.0056 & 1.0000 & -0.0015 \\ 0.0002 & 0.0015 & 1.0000 \end{bmatrix} \quad (15)$$

After optimising the global calibration of the fused point clouds P_{21}, P_{34} with the calculation results of the above formulae, the four measurement units were re-scanned for cylindrical pieces, and the accurately stitched cylindrical point cloud model is shown in Fig. 11.

From Fig. 11, it is easy to see that the cylindrical point cloud data after secondary calibration does not show the phenomenon of point cloud splicing and layering, which indicates that the global calibration optimisation method proposed in this paper is very reliable.

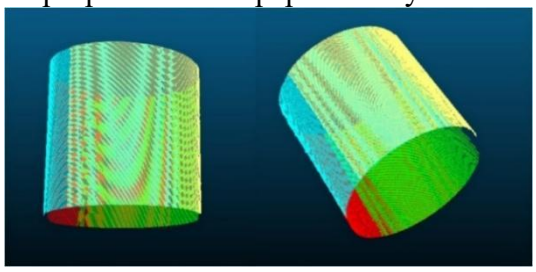

Figure 11: Results after global calibration optimization

4.2 Measurement system accuracy verification

In order to further quantitatively analyse the measurement accuracy of the multi-view line structured light 3D measurement system proposed in this paper, a system accuracy evaluation system is established. In this paper, a standard block with dimensions of 60mm×35mm×9mm as shown in Fig. 12 is used for the accuracy evaluation experiments, in which the block is fixed on a mobile platform, and the four line-structured light measurement units scan the standard block sequentially. In order to reduce the chance error of the measurement system, five sets of measurement experiments will be carried out, and the position of the block in the measurement system will be changed continuously during the experiments, and the root-mean-square error between the measured values of the block's length, width, and height and the standard values will be calculated to represent the measurement accuracy of the whole system.

Figure 12: Standard blocks

(a) Point cloud data acquired in each view point (b) Stitched point cloud data

Figure 13: Block Scanning Results

As shown in Fig. 13(a) for the volume block point cloud data acquired by the four line structured light measurement units in one set of experiments, after point cloud stitching and global optimisation, the standard volume block point cloud data is shown in Fig. (b). The length, width and height of the block point cloud are measured using the 3D point cloud processing software Cloud Compare, and the measured values of the block dimensions are obtained as shown in Table 2.

Table 2: Measured values of gauge block dimensions

experimental group	gauge	error value	gauge width	error value	gauge height	error value
1	60.0427	0.0427	34.9638	0.0362	8.9421	0.0579
2	59.9773	0.0227	34.9832	0.0268	9.0438	0.0438
3	60.0473	0.0473	35.0471	0.0471	8.9636	0.0364
4	60.0387	0.0387	34.9538	0.0462	8.9438	0.0562
5	59.9626	0.0374	35.0313	0.0313	9.0446	0.0446
RMS		0.0387		0.0384		0.0485

From the analysis of the above table, it can be seen that the overall measurement error of the multi-view line structured light 3D measurement system constructed in this paper is less than 0.05mm. This measurement result also indicates that the point cloud data stitching accuracy of this paper is high, and the four local line structured light measurement units also have high measurement accuracy. Therefore, the measurement system built in this paper can meet the high-precision measurement requirements and can be used to measure the blade surface profile.

4.3 Aero-engine blade measurement experiment

In order to verify the feasibility and effectiveness of the proposed method in practical applications, the aero-engine turbine blades are scanned using the constructed multi-view line structured light 3D measurement system, as shown in Fig. 14.

Figure 14: Blade appearance

The local measurement data collected by the multi-view line structured light 3D measurement

system are shown in Figs15. (a)~(d), and the local measurement point cloud data are spliced and fused based on the global calibration and global optimisation results, and the results are shown in Fig. 16.

Using high-precision measuring equipment optical image measuring instrument scanning to obtain the experimental sample blade surface 3D data, the collected data as the theoretical model of the blade, and the global splicing of the experimental sample shape data for the alignment of the alignment, the results are shown in Figure 17. The standard deviation of the blade is 0.1253mm, which meets the measurement requirements of the blade profile, and verifies the reliability and validity of the global calibration method proposed in this paper, as analysed by CloudCompare software.

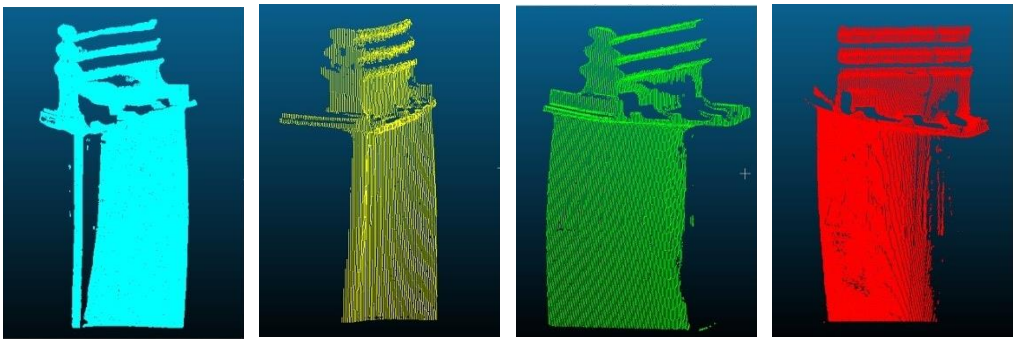

Camera 1 view to acquire point cloud | Camera 2 view to acquire point cloud | Camera 3 view to acquire point cloud | Camera 4 view to acquire point cloud

Figure 15: Point clouds obtained from each viewpoint

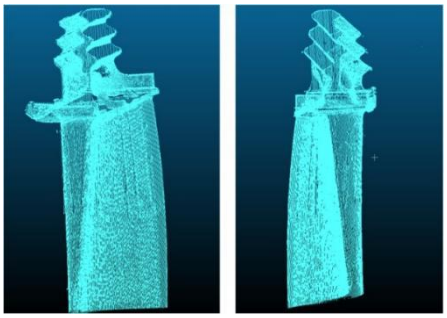

Figure 16: Point cloud model after global stitching

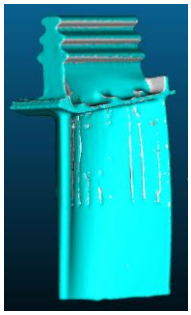

Figure 17: Blade model comparison results

5. Conclusions

Aiming at the requirement that the existing blade line structured light three-dimensional measurement method cannot take into account the measurement accuracy and the measurement integrity, a multi view line structured light 3D measurement system was constructed using four industrial cameras and two line lasers, and a high-precision point cloud global splicing method was proposed to achieve accurate measurement of the entire surface of aircraft engine blades. The experimental results show that the average standard deviation of this paper's method for the blade is 0.1253mm, which meets the actual detection requirements. From the analysis of experimental measurement results, the method proposed in this paper has the advantages of high measurement accuracy, large measurement range and low cost, and the method is proved to be feasible through experiments.

References

[1] Yao Meiru. Research on three-dimensional visual measurement technology of aero-engine blade face shape [D]. Harbin Institute of Technology, 2019.

[2] Han Ruilu. Research on key technology of three-dimensional reconstruction and defect detection of aero-engine blade-like parts [D]. North University of Technology, 2021.

[3] Shi Xiaoqiang, Wu Baohai, Zhang Dinghua. Development status and trend of aero-engine blade processing quality inspection technology [J]. Aviation manufacturing technology, 2015(12):80-84.

[4] Boyce M P.Gas turbine engineering handbook [M].Oxford: Butterworth-Heinemann.2011.

[5] Duo Li, Bo Wang, Zhen Tong, Liam Blunt, Xiangqian Jiang. On-machine surface measurementand applications for ultra-precision machining: a state-of-the-art review [J]. International Journal of Advanced Manufacturing Technology, 2019, 104: 831-847.

[6] Li Xuezhe, Shi Zhaoyao, Chen Hongfang, et al. Research status and trend of aero-engine blade profile measurement technology [J]. Journal of Beijing Institute of Technology, 2017, 43(4):557-565

[7] Huang Z, Li K, Zhao L, et al. Current status and development trend of optical measurement technology for aero-engine blade profile D]. Aviation manufacturing technology, 2018, 61(22):28-35.

[8] Cai Jingyi. Research on multi-view 3D reconstruction technology based on coded structured light [D]. Nanjing University of Information Engineering, 2021.

[9] Ge Qingru. Research on three-dimensional measurement technology of high-speed railway body-in-white based on multimetric vision line structured light [D]. Huazhong University of Science and Technology, 2020.

[10] Wei Xiaoxin. Research on multi-view 3D reconstruction and stitching method based on line structured light [D]. Tianjin University of Technology, 2021.

[11] Xu Pei. Research on multi-view automatic stitching algorithm of structured light 3D scanning system [D]. Guilin University of Electronic Science and Technology, 2019.

[12] Chen M, Tang Y, Zou X, et al. High-accuracy multi-camera reconstruction enhanced by adaptive point cloud correction algorithm [J]. Optics and Lasers in Engineering, 2019, 122:170-183.

[13] Huang L, Da F, Gai S. Research on multi-camera calibration and point cloud correction method based on three-dimensional calibration object [J]. Optics and Lasers in Engineering, 2019, 115:32-41.

[14] W. Sun, H. Yuan, N. Liu, R. Liu, and S. Shu. A fast alignment algorithm for line laser point cloud fusing contour features [J]. Journal of Electronic Measurement and Instrumentation, 2021, 35(07):156-162.

[15] Zhang Z. A flexible new technique for camera calibration [J]. IEEE Transactions on pattern analysis and machine intelligence, 2000, 22.